Bow Spring/Tendon Actuation for Low Cost Haptic Interfaces*

DALE A. LAWRENCE† LUCY Y. PAO§ SUTHA APHANUPHONG†

†Aerospace Engineering, University of Colorado, Boulder, CO 80309–0429
§Electrical Engineering, University of Colorado, Boulder, CO 80309–0425
E-mail: dale.lawrence@colorado.edu, pao@colorado.edu, sutha.aphanuphong@colorado.edu

Abstract

This paper describes a novel bow spring and tendon actuator design for a haptic interface that provides high-bandwidth force transmission to the fingers, with a large range of motion. This is combined with a low-cost stepper motor and a low-cost optical encoder, along with self-calibration and control compensation to produce a smooth force source with excellent hard virtual wall rendering capabilities. Four techniques are discussed to compensate for bow spring, friction, and ripple torques in the actuator. Experimental results quantify the achieved force rendering quality of each technique, and provide a measure of hard virtual surface rendering quality in one degree of freedom.

1 Introduction

Haptic interfaces have been in use for over 40 years in a number of applications, ranging from force-feedback teleoperation systems to scientific data visualization to virtual training systems. Due to the variety of applications, haptic interface designs span a wide range, from interfaces with non-dextrous, power grips to many recent haptic interface designs with more sensitive and dextrous finger grips [3, 4, 7, 9, 17]. The primary technical difficulty in all these designs is providing accurate, high frequency force information to the user, in multiple degrees of freedom, and with large range of motion. This poses unique challenges in mechanism and control design [1, 3, 4, 5, 7, 9, 12, 16, 17, 21]. To achieve hard "crisp" surfaces needed in many haptic interface applications [5, 11], smooth velocity measurements with small computational delay are required [13]. This is often provided via position sensing, resulting in requirements for position sensor resolution that far exceed what users can kinsthetically distinguish. High bandwidth force transmission to the fingers requires a lightweight, stiff transmission, and a low mass actuator with high force capability and low friction and ripple forces.

*This work was supported in part by the U. S. National Science Foundation (HRD-0095944).

We previously described a motor and encoder approach [13] for haptic interfaces aimed at achieving these design objectives while keeping hardware costs to a minimum. The design uses a low-cost stepper motor and a low line-count optical encoder, together with high speed digital signal processing to achieve high torque levels with low ripple, as well as high-resolution position and velocity sensing. While this approach requires more involved electronics and signal processing, these components see wide use in other high-volume products, resulting in steeper cost reductions compared to motors and sensors. We believe this approach will lead to high performance haptic interfaces which are significantly lower in cost.

In this paper, we combine the stepper motor and encoder with a new bow spring and tendon design that provides a compact, large range of motion prismatic actuator. Section 2 describes the bow and tendon concept. Section 3 briefly reviews the motor and encoder design and pulse width modulation scheme presented in [13]. In Section 4, we describe a combination of several actuator compensator methods that can significantly improve the quality of force rendering. Experimental results from implementing these control methods are provided in Section 5.

2 Bow & Tendon Design

Figure 1 shows a photograph of the prototype bow spring/tendon device, and Figure 2 illustrates the distal and proximal limits on the range of prismatic motion. Forces are transmitted to the stylus by varying tension forces in the thin, stainless steel tendon (76μm by 2.5 mm) connecting the motor to the stylus. The tendon is lightweight yet very stiff in tension. The bow spring is a length of 1.25 mm diameter music wire that provides a preload of approximately 5 N in the tendon, enabling bi-directional forces up to $\pm$5N to be transmitted to the user. The tendon is simply wrapped on a 22.8 mm diameter pulley to convert motor rotation to prismatic motion. As discussed in [13], the stepper motor is capable of relatively large torques due to its many, closely spaced salient poles (50 per

Proceedings of the First Joint Eurohaptics Conference and Symposium on Haptic Interfaces for Virtual Environment and Teleoperator Systems
0-7695-2310-2/05 $20.00 © 2005 IEEE

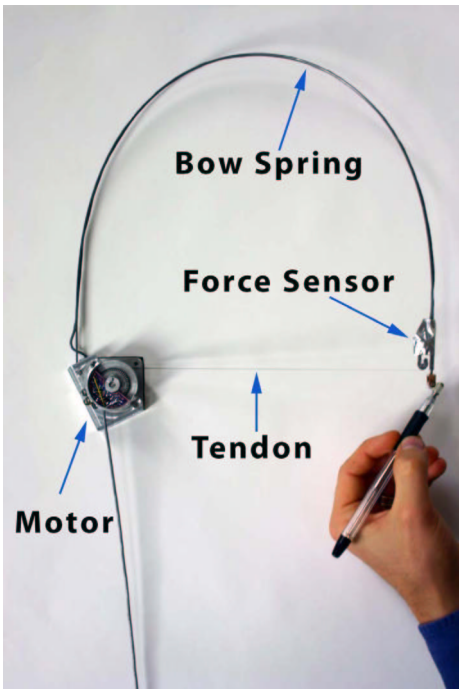

Figure 1: Bow spring and tendon actuator prototype shown in mid extension. Total prismatic range of motion is 40 cm.

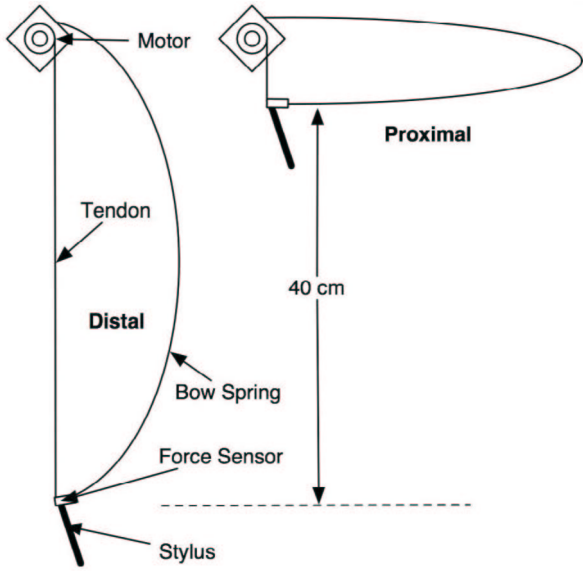

Figure 2: Bow spring and tendon actuator at distal and proximal extremes of its range of motion.

mechanical turn), so gear reduction is not required. This "electromechanical gearing" enables a stiff, low friction, zero backlash transmission from electromechanical torque to the forces on the user's fingers.

Several of these one degree of freedom (DOF) actuators can be attached to a haptic interface grip (e.g., a stylus) to produce a parallel, multi-DOF interface, e.g., as in the rod-based parallel interface [14]. This idea of transmitting forces via tendon tension is similar to cable-actuated devices (see e.g., [22] for a description of several types), except that the current approach does not require opposing cables, using the bow spring instead to ensure each cable (tendon) is always in tension. This results in a much more compact interface, which the user does not have to reach into, and range of motion is increased due to lack of interference with actuating/tensioning cables.

The motor is mounted to the interface base via a pivot shaft, whose axis of rotation is in the plane of the actuator pulley. This provides two degrees of freedom in rotation (about the pivot axis and the motor shaft) at the actuator base. Together with the prismatic degree of freedom in the tendon itself, a three-degree of freedom gimbal is used at the stylus connection to enable six degrees of freedom in stylus motion, with only the prismatic DOF active in each actuator. The bow spring is attached so that the motor aligns the tendon on the pulley as the user moves the stylus throughout the workspace. The current prototype has a prismatic motion range of 40 cm, an angular motion range at the base attachment of 180 degrees about the pulley axis, and unlimited rotation about the pivot.

Note that the bow spring does not project behind the actuator, but does bend outward as the actuator is moved proximally. The actuators must be arranged so that the bow spring does not contact those of other actuators or the user's hand. For example, if all actuators are oriented so that the bow springs remain in a vertical plane, interference is avoided by the angular offset between actuators.

3 Motor & Encoder Design

A new stepper motor drive was presented in [13] that uses an inexpensive low-resolution optical encoder to electrically commutate a stepper motor, producing high torque levels with low ripple. Compared to a number of motor options [13], the hybrid stepper motor provides significantly reduced moving mass for the same torque and motor temperature while having a small overall actuator mass.

Figure 3 shows a close-up of the prototype stepper motor and encoder. The motor body is 42mm $\times$ 42mm $\times$ 34mm. The encoder disk is 25mm in diameter, and the low cost reflective optical sensor electronics are visible in the figure, along with slots containing spiral bands for soft-stop limiting of motor rotation to 6 total revolutions.

This hybrid step motor uses the common arrangement of 200 steps per turn, resulting from 50 pole teeth: 4 steps per pole $\times$ 50 poles per mechanical turn. Due to mechanical imperfections in manufacturing the teeth of the rotor and stator poles, the torque τ developed in the motor is only approximately sinusoidal. Thus, the actual torque produced by the motor consists of sinusoidal components, plus a ripple torque τ_R which is a function of both rotor-stator angle and coil current.

Proceedings of the First Joint Eurohaptics Conference and Symposium on Haptic Interfaces for Virtual Environment and Teleoperator Systems
0-7695-2310-2/05 $20.00 © 2005 **IEEE**

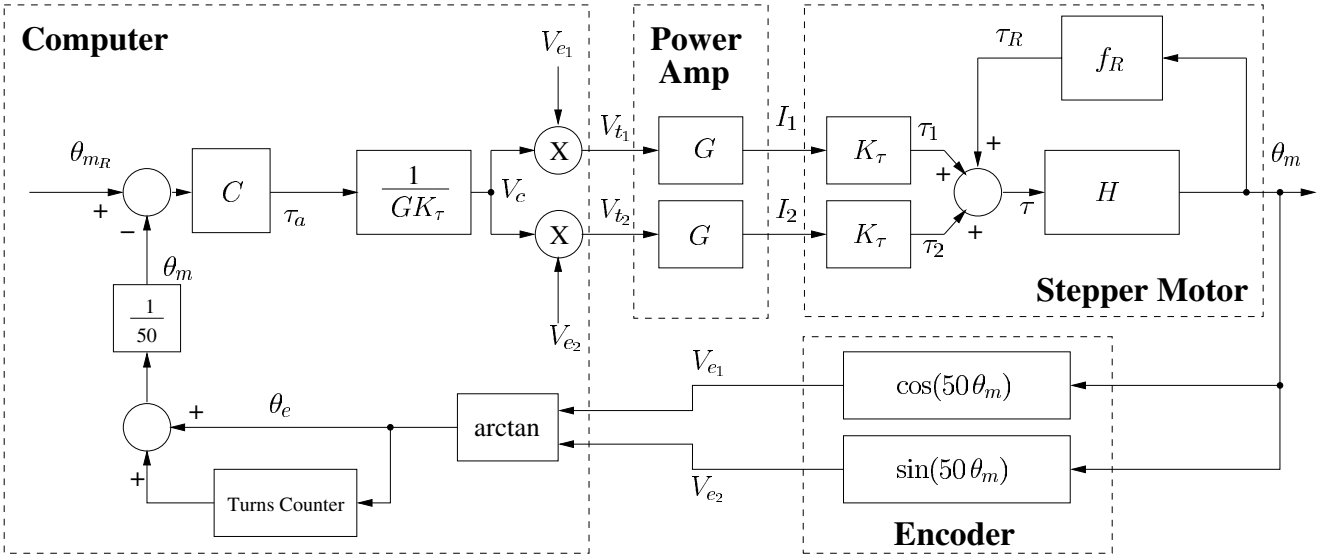

Figure 4: Control loop used to commutate the motor and measure ripple and friction torques for subsequent compensation.

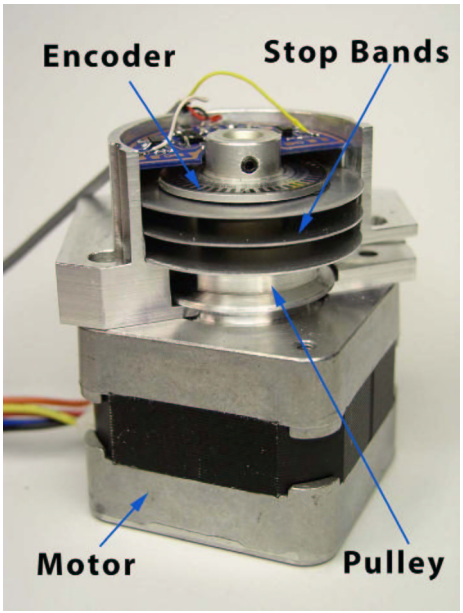

Figure 3: Stepper motor and low line-count encoder.

We employ sine wave commutation, illustrated in Figure 4, requiring that the angular position of the rotor be known to a small fraction of an electrical turn so that smooth sinusoidal motor current results. Further, we also want to cancel the friction and ripple torques τ_R, which are the differences between the actual torques and the assumed sinusoidal torques. This requires that additional feedback torque be provided (see Section 4.3) that is a function of rotor position. We did not address the friction components in our previous work, and these are discussed in Section 4.2. Our approach is simpler than the adaptive methods of [2, 18], using straightforward spline fitting and interpolation methods on measured data.

The optical encoder scheme that we use [13] produces an analog output instead of a digital quadrature output. By choosing the optical and electrical parameters appropriately, it is possible to produce a pair of quadrature voltages that are approximately sinusoidal functions of rotor position, periodic on the angular spacing of the optical stripes on the encoder disk. While many different optical periods could be used, it is most convenient for commutating the motor to match the optical and electrical periods, so the encoder signals have the same period as the motor quadrature torques. In our design, this requires only a 50 line optical encoder disk that can be small and inexpensive to produce.

While not necessary for commutation, position sensing resolution of 1 part in 1000 on an electrical turn is easy and inexpensive to provide by using at least a 10 bit A/D converter on the encoder signals, yielding an angular position sensing resolution of 1 part in 50,000 on one mechanical turn. With a direct drive pulley radius of 11.4 mm, the prismatic actuator sensing resolution is 1.4 μm, which is approximately that required in haptic interface applications where hard virtual surfaces are rendered [13].

The sine wave commutation/encoding approach enables low cost motor and encoder hardware to be used, but has consequences in electronics and signal processing that must be appreciated. In particular, higher bandwidth and higher voltage drivers as well as higher sample rates in the commutation controller are needed. While this increases overall cost, the cost of these electronic components in the design have been continuously decreasing, due to high volume production for a variety of other applications.

Proceedings of the First Joint Eurohaptics Conference and Symposium on Haptic Interfaces for Virtual Environment and Teleoperator Systems
0-7695-2310-2/05 $20.00 © 2005 **IEEE**

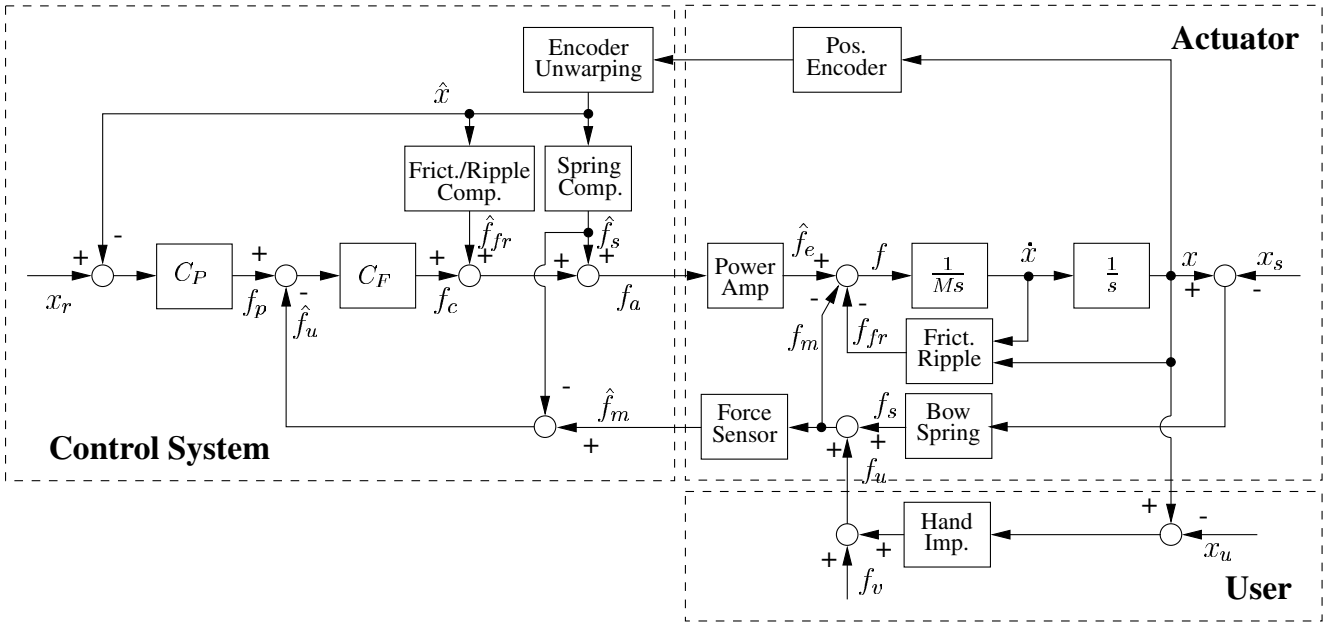

Figure 5: Overall block diagram of the tendon bow actuator control system, indicating feedback of both motions and forces to compensate for bow spring bias, step motor friction, and step motor ripple forces.

The stepper motor has a torque constant $K_\tau = 0.17$ Nm/A, resulting in high torque and correspondingly high back EMF ($K_{EMF} = 0.17$ V/rad/sec). The stepper motor avoids the cost, friction, backlash, and inertia effects of a gear head by utilizing its "electromagnetic gearing". The downside of this gearing is the need to provide higher voltages in the motor driver to overcome the larger back EMF. The motor winding inductance requires that the driver voltage increase with commutation frequency if the desired current is to be supplied. If the voltage rails in the driver are too small, the current becomes slew-rate limited at high frequencies and high amplitudes, becoming another source of reduced current and miscommutation.

In our design, we desire a maximum prismatic actuator force of 10 N at a maximum speed of 1 m/s. With a simple pulley converting rotary to prismatic motion, and a pulley of radius 11.4 mm, we require full scale torques of τ_m = 0.11 Nm to be supplied up to a shaft speed of $\omega_m = 87$ rad/sec, or an electrical turn frequency of 4350 rad/sec. With an armature resistance R of 8 Ω and an inductance L in each motor coil of 10 mH, this implies that a driver capable of supplying 48 V at 0.65 A is needed [13].

A pulse-width-modulation (PWM) driver provides an efficient solution. By controlling the average on-time in MOSFET switches, the average current over a switch cycle can be accurately controlled, with very little dissipation in the power driver. The driver dissipation is actually primarily driven by the PWM switching frequency, since significant instantaneous power is dissipated over several tens of nanoseconds as the drivers pass from the fully off to the fully on state. The PWM board we developed [13] is 43 mm × 48 mm × 7 mm and can deliver a full scale current of ±0.65 A at any voltage up to ±60 V with approximately 2 W total dissipation, requiring no additional heat sink. It switches at 100 kHz, has a small signal current loop bandwidth of 30 kHz, and a slew rate of 6000 A/sec into a 10mH inductive load. Full scale sinusoidal current bandwidth is 2 kHz. It uses standard, high volume production components to result in a low cost, compact driver.

4 Actuator Compensation

This section discusses several types of compensation employed by the control system to ameliorate residual force defects in the hybrid stepper motor and the tendon/bow conversion of rotary to prismatic actuation. Figure 5 shows the structure of the control system with the commutation detail of Figure 4 suppressed. Also, all variables are converted from rotational to their equivalent translational (prismatic) values.

4.1 Bow Spring Compensation

The bow spring provides the bias force necessary to achieve bidirectional actuation forces by varying tension in the tendon around the bias force. An accurate prediction of the proper bias force is required so that the motor can balance the spring force, preventing the user from feeling this spring as the stylus is moved throughout its range of

Proceedings of the First Joint Eurohaptics Conference and Symposium on Haptic Interfaces for Virtual Environment and Teleoperator Systems
0-7695-2310-2/05 $20.00 © 2005 IEEE

motion. The control system estimates the bow spring deflection force f_s at each time sample k as a simple affine function of estimated instantaneous position $\hat{x}$:

$$\hat{f}_s(k) = f_0 + K_s\hat{x}(k) \quad (1)$$

The data for this model is obtained in a self-calibration process, where the position control loop in Figure 5 is used to place the actuator at a series of positions, measuring the actuator forces f_a necessary to hold each position. Figure 6 shows the measured force data as a function of spring deflection range, along with the simple affine curve fit used to calculate on-line bias forces $\hat{f}_s(k)$. Note that the average spring force appears linear with deflection over the 23 cm prismatic range of motion shown. Model parameters are $K_s = 9.3$ N/m and $f_0 = -6.0$ N.

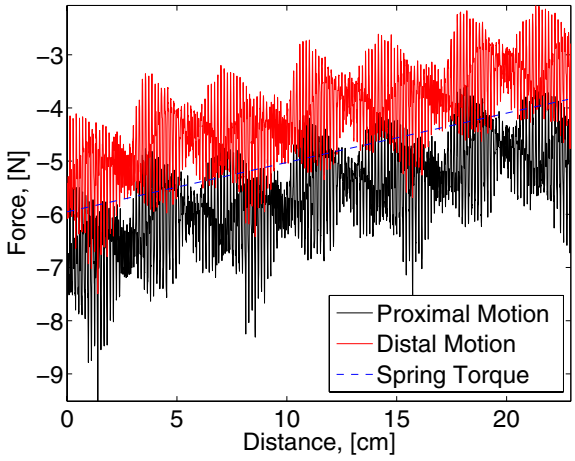

Figure 6: Force produced by the position control system as a function of prismatic range of motion, showing a pronounced linear spring effect.

When this spring model is applied as shown in the block diagram of Figure 5, no spring forces can be felt by the user, and when the stylus is released, the actuator remains at that position, indicating that the spring forces are accurately compensated by this term in the control system.

4.2 Friction Compensation

When the bow spring forces have been neutralized, significant resistance can still be felt as the stylus is moved. Both force ripple and friction-like forces are present. This section addresses the friction forces. When the spring force $\hat{f}_s$ is removed from the force f_a required to hold various positions, the forces shown in Figure 7 result.

Two different offsets are apparent in the data, corresponding to the direction of travel in the data collection experiment. This would suggest the presence of a Coulomb friction characteristic. Indeed, as the stylus is moved by the user, the opposing force rapidly changes sign as the

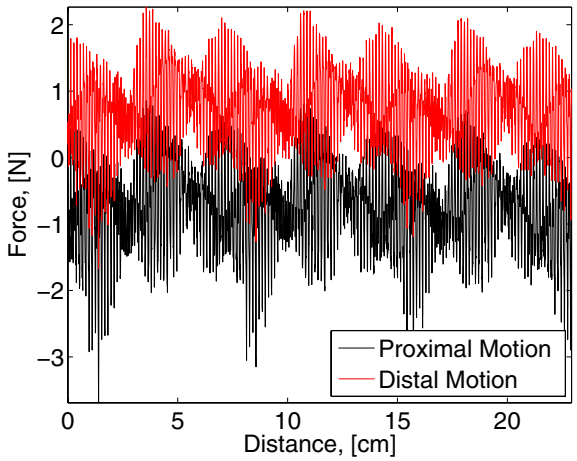

Figure 7: Force versus distance with spring forces removed shows a directionally dependent friction force, and noticeable force ripple.

direction of travel is reversed. This can be seen by measurements of the user's interaction force as a function of position, as shown in Figure 12 later. Neutralization of this effect would seem to require a control force as indicated in Figure 8.

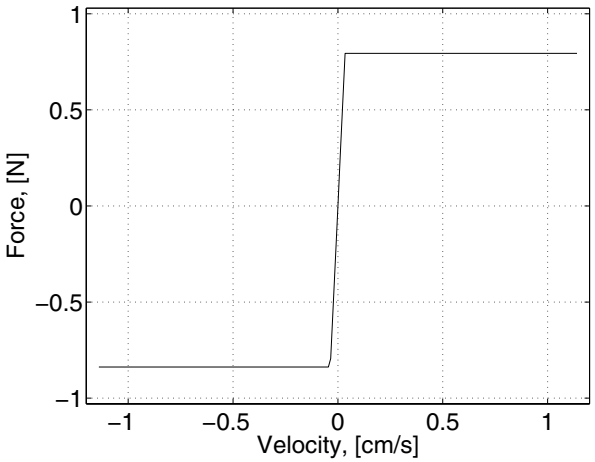

Figure 8: Classical Coulomb friction characteristic with a finite (but large) slope near zero velocity.

Unfortunately, the large slope near zero translational velocity in this function amounts to a large feedback gain which interacts with delay in the digital implementation to produce instability. A typical recourse is to reduce the slope until stability is recovered. However, this leaves the initial "edge" in the friction characteristic uncompensated, resulting in a more pronounced stick-slip feeling where stylus velocity is small. In this work, we have explored an alternative utilizing a hysteretic friction model, which al-

Proceedings of the First Joint Eurohaptics Conference and Symposium on Haptic Interfaces for Virtual Environment and Teleoperator Systems
0-7695-2310-2/05 $20.00 © 2005 IEEE

lows steeper slopes in the friction characteristic to be used due to its stability enhancing energy loss.

We employed a "velocity mode" hysteretic compensation, as illustrated in Figure 9. This is implemented using

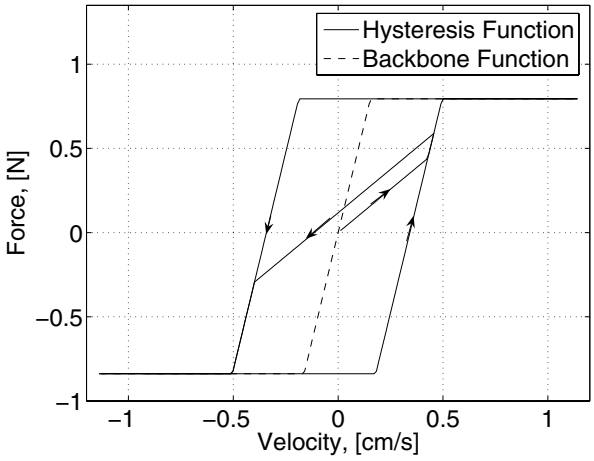

Figure 9: Velocity mode friction compensation utilizes a simple saturation function as a backbone, and adds hysteresis via a simple slip-state offset in the function argument.

a simple "slip-state" modification of a backbone function F (dashed line in Figure 9). This technique is similar to the Maxwell friction model used in [15], which is much simpler than the popular Preisach model [10, 8] or the generalized Maxwell model [6]. The compensation force f_f is found from the following:

$$f_f = F(\dot{x} - s) \tag{2}$$

Here, the slip state s follows the translational velocity $\dot{x}$ in the center region in Figure 9 where hysteretic energy loss occurs, resulting in little change in f_f. In contrast, s becomes fixed at higher velocities, so that the compensation forces follow the backbone function F. The slip state is specified as follows:

```
if ẋ(k) − ẋ(k−1) > 0, then (ẋ is increasing)
    s(k+1) = s(k) + α ∗ (ẋ(k) − ẋ(k−1))
        (Increment is proportional to change in
    translational velocity)
    if s(k+1) > s_max, then
      s(k+1) = s_max
            (Slip state is saturated at s_max)
    endif
endif

if ẋ(k) − ẋ(k−1) < 0, then          (ẋ is
    decreasing)
    s(k+1) = s(k) + α ∗ (ẋ(k) − ẋ(k−1))
        (Increment is proportional to change in
    translational velocity)
    if s(k+1) < s_min, then
      s(k+1) = s_min
            (Slip state is saturated at s_min)
    endif
endif
```

This approach not only provides the large hysteresis loop behavior, but enables suitable small-loop behavior (e.g. as shown in the figure) to be specified with very small computational and memory requirements.

The upper and lower saturated levels of the backbone function f_U and f_L are found by averaging the force data in each direction shown in Figure 7. When applied in the compensation control, significant reduction in the stick-slip feeling relative to the non-hysteretic approach can be obtained without causing instability, by adjustment of the parameters α, s_{max}, s_{min}, and the slope β of the backbone function. We used $\alpha = 0.85$, $s_{\max} = -s_{\min} = 0.34$ cm/s, and $\beta = 520$ Ns/m. The resulting stick-slip effect is absent at some translational positions, but remains at others. This variation is due to the effects of ripple force, which accentuate the forces required to cause motion where the ripple potential wells are more severe. Force ripple can be effectively removed by a simple modification of the velocity mode friction compensation, as discussed next.

4.3 Force Ripple Compensation

Departure from pure sinusoidal force profiles in the commutation cycle produces unwanted ripple or cogging force f_r. This is caused by tooth profiles in the stator and rotor not being optimized for sinusoidal torque, by variation from tooth to tooth due to manufacturing tolerances, and by errors in the position measurement within the commutation cycle due to imperfect sinusoidal encoder signals.

As seen in the close-up of the f_a data (with spring forces removed) in Figure 10, the ripple forces are similar in each direction, but differ in detail. Further, ripple differs over each electrical turn, due to the slight differences in magnetic properties among the motor rotor and stator poles. There are 50 poles in this hybrid step motor, yielding 50 electrical turns per mechanical turn. In addition, the ripple differs in each mechanical turn due to the larger current required to oppose the bow spring as it is compressed toward its proximal limit.

A cubic spline is fit to this data, with control point spacing which can capture most (but not all) of the ripple characteristic. This is a trade-off between accurate ripple compensation on the one hand, and measurement noise smoothing and reasonable data storage for real-time interpolation on the other hand. We found a control point spacing of 10 points per electrical turn to be adequate.

Separate splines are fit to the proximal and distal motion directions, allowing approximate ripple torques f_{rp} and f_{rd} to be interpolated from the splines at any translational position x, depending on motion direction. These

Proceedings of the First Joint Eurohaptics Conference and Symposium on Haptic Interfaces for Virtual Environment and Teleoperator Systems
0-7695-2310-2/05 $20.00 © 2005 IEEE

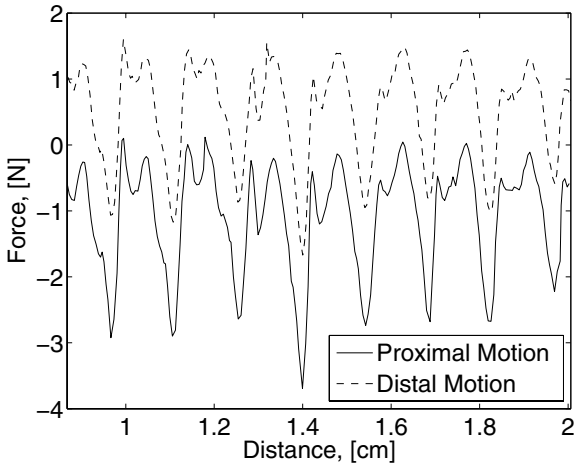

Figure 10: Close-up of the measured force ripple shows variations between electrical turns, as well as a dependence on motion direction.

functions are then used to define the friction compensation backbone function upper and lower saturation limits, i.e.,

$$f_U = f_{rd}(x)\ ;\ f_L = f_{rp}(x) \tag{3}$$

making the friction compensation a function of both velocity and position. This is very effective in neutralizing the feeling of both friction and ripple when the stylus is moving. (See the force data and discussion in Section 5). However, stick-slip edges can still be felt as the stylus is moved from some stopped positions.

4.4 Force Feedback

Despite significant reduction in friction effects from the velocity mode friction and ripple compensation terms, stick-slip edges can still be perceived. Actually, this feeling is accentuated by good friction compensation, since all other anomalies have been removed, leaving only the slight differences between the mechanical friction and its compensation near zero velocity. The fingers are exquisitely sensitive in the stylus grip, making it very difficult to remove this effect using a feedback of sensed motion. Essentially, this type of model cannot produce a compensation force until a sufficient motion occurs, but perceptible forces are required to cause this motion. These remaining friction effects can only be addressed by providing a compensation force which is proportional to the forces produced by the user, i.e., a compensation force which can occur *before* sufficient motion occurs. User interaction forces cannot be predicted, hence must be directly measured near the point where the stylus is connected to the bow/tendon actuator. Figure 11 shows a prototype force sensor, which measures the tension in the tendon via strain gages.

Static tendon tension is the difference between the bow spring force and the user's interaction force. Dynamic tensions involve the forces necessary to accelerate the mass of the force sensor, bow spring, and stylus. However, these components are small and lightweight, and force feedback compensation is needed only for slow motions that occur in the neighborhood of a fixed stylus position. For these motions, accelerations are negligible, and the difference $\hat{f}_u$ between the modeled bow spring torque $\hat{f}_s$ and the measured tendon tension $\hat{f}_m$ provide a suitable measure of user interaction forces for compensating the remaining stick-slip effects.

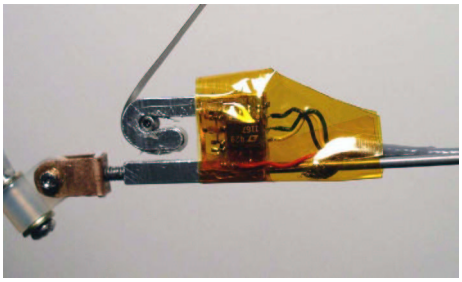

Figure 11: Miniature force sensor developed for the tendon bow actuator measures tendon tension for residual stick-slip friction compensation.

The user interaction force feedback is implemented in a force control loop, where a lag-type controller is applied to the difference between the desired (or commanded) actuator force f_p and the measured interaction force $\hat{f}_u$, i.e.,

$$f_c = \left(K_p + \frac{K_i a}{s+a}\right)(f_p - \hat{f}_u) \tag{4}$$

as shown in Figure 5. This controller produces a large gain $K_p + K_i = 11$ at frequencies below $a = 2$ rad/sec, and a smaller gain K_p (set to one here) at high frequencies. Thus, only the slow, small motions are significantly affected by the force feedback, leaving the motion-dependent force models to provide friction and ripple compensation for all other motions. This enables low feedback gains to be applied in the force loop at high frequencies, which enhances stability robustness to variation in user grip strength, attachment of multiple actuators together for multi-DOF actuation, etc. The next section compares the performance obtained from these compensation methods.

5 Experimental Results

This section discusses experimental results obtained with the compensation methods from the previous section. First, free space motion is evaluated by measuring the forces required to move the stylus under two types of motions. The first motion is slow, covering a displacement of approximately 8 cm in sinusoidal-like motions with a

Proceedings of the First Joint Eurohaptics Conference and Symposium on Haptic Interfaces for Virtual Environment and Teleoperator Systems
0-7695-2310-2/05 $20.00 © 2005 IEEE

period of about 5 sec. This results in peak velocities of about 3 rad/s. Slow motions exhibit ripple and residual "edges" from friction compensation more clearly. The second type of motion is faster, covering an 8 cm displacement in about 2 sec., resulting in peak actuator angular velocities of about 9 rad/s. Faster motions exhibit the effective mass of the interface more clearly. Since the force sensor measures tendon tension, external (user) forces f_u necessary to cause motion are computed as the difference between the measured sensor tendon force $\hat{f}_m$ and the predicted spring force $\hat{f}_s$. The force ($\hat{f}_u$) versus displacement ($\hat{x}$) data constitutes a measure of the haptic interface mechanical impedance felt by the user at the frequency of motion. For a given motion, these forces provide a measure of the mass, friction, and ripple residuals of the compensation, and are one means of quantifying the transparency [5, 11] of the interface.

Next, the performance of the one-DOF interface is evaluated in its rendering of hard virtual surfaces. A linear spring and one-way damper model is used for the virtual surface, and measurements of the force rate of change versus the position rate of change are made. This "rate-hardness" characteristic has been shown to be an important indicator of the quality of virtual surfaces [11].

5.1 Force vs. Distance: Slow Motions

Figure 12 shows all four compensation effects on common scales, for one cycle of the slow voluntary motion. Plot (a) is the result of using only the bow spring compensation. Note the force has a different offset between proximal and distal motion, characteristic of Coulombic-type friction, together with significant ripple forces. The feel of the interface is poor, producing noticeable resistance to motion, and annoying ripple forces. It is particularly difficult to move the interface at slow, constant speeds.

Plot 12 (b) is the result of combining bow spring and friction compensation methods. This removes the offsets in the interaction forces, allowing nearly effortless higher-speed motion, although force ripple is still noticeable, which still prevents slow constant-speed motion. In addition, the "edge" that opposes motion direction changes is even more apparent than in plot (a), due to the now larger contrast between static and dynamic friction values.

Plot 12 (c) adds ripple compensation to part (b), significantly reducing forces. This makes the interface feel very smooth for motions away from zero velocity. Ripple is still apparent if the user looks for it, but it is apparently very near the perceptual threshold, and is no longer distracting. However, when changing direction while moving very slowly, the user is still able to feel a stick-slip "edge" (note the spike in force at the left extreme in plot (c)), which is now the most apparent flaw in the interface.

Finally, plot 12 (d) shows the result of combining bow spring, friction, ripple, and a force feedback compensator in the control system. This has an imperceptible effect on most of the slow motion forces, but does improve the stick-slip "edge" considerably. Now, very slow motion can be produced, including fine control over changes in direction. In some places (but not all), the "edge" has been completely removed.

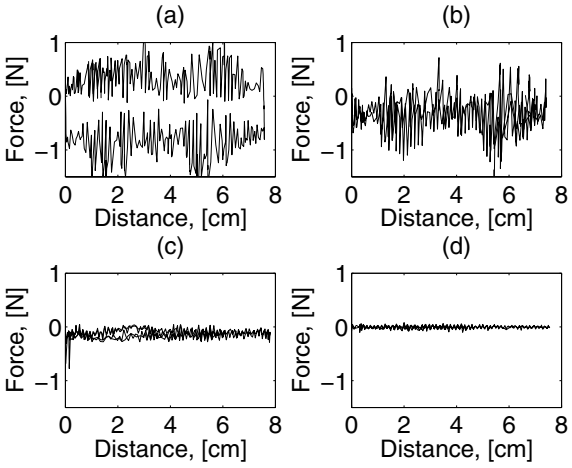

Figure 12: Interaction force $\hat{f}_u$ versus distance $\hat{x}$ for slow voluntary motion: (a) only spring compensation, (b) spring and friction compensation, (c) spring, friction, and ripple compensation, (d) spring, friction, ripple, and force feedback compensation.

5.2 Force vs. Distance: Fast Motions

Plot 13 (a) shows force versus distance applying only bow spring compensation, for seven cycles of the fast motion. Comparing this with Figure 12 (a), fast motions produce less apparent ripple than slow motions. This is believed to be due to the filtering effect of the mass in the actuator, and distal parts of the bow, together with the compliance of the tendon. Faster motions produce higher frequency ripple forces, which are mechanically attenuated before they arrive at the users fingers (or the force sensor). This effect is also perceptible: fast motions feel much smoother. Plot 13 (b) shows the results of adding friction compensation to the control system. As before, this significantly reduces the force needed to move the actuator. Plot 13 (c) shows the results with ripple compensation added to the control system. This is very effective for faster motions, making the interface feel quite smooth. For this motion, the "edge" near motion direction change is less apparent than for slow motions, but still noticeable. Adding force feedback produces the forces shown in plot 13 (d). The measured forces are larger here than for the slow motions due to the acceleration of the effective mass of the interface, but the effective mass has also been reduced by the force feedback (compare plot (c) and plot (d)).

Proceedings of the First Joint Eurohaptics Conference and Symposium on Haptic Interfaces for Virtual Environment and Teleoperator Systems
0-7695-2310-2/05 $20.00 © 2005 **IEEE**

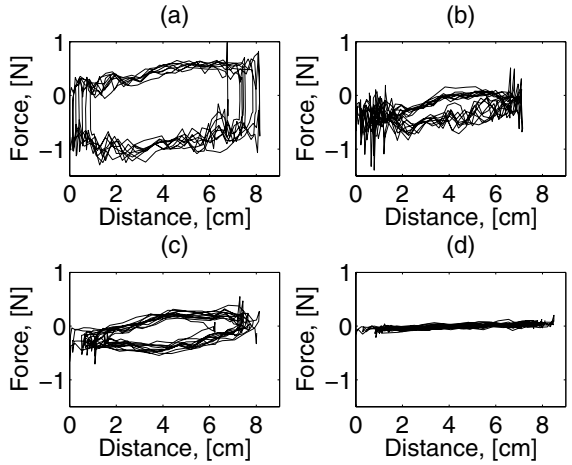

Figure 13: Interaction force versus distance for fast voluntary motions: (a) only spring compensation, (b) spring and friction compensation, (c) spring, friction, and ripple compensation, (d) spring, friction, ripple, and force feedback compensation.

5.3 Hard Virtual Wall Performance

A virtual surface was created at a position x_w near the distal end of travel, produced by forces f_w following a simple spring/damper model

$$f_w = -k_w(x - x_w) - b_w(\dot{x} + |\dot{x}|)/2 \qquad (5)$$

when $x - x_w$ is positive (stylus position is inside the virtual wall), and zero otherwise. Note that the damping effect is only applied when penetration distance is increasing (when $\dot{x}$ is positive). This prevents the surface from feeling "sticky" as the stylus is withdrawn from the surface. As in all the data taken in this paper, the control loop runs at a sampling rate of 9.09 kHz. As suggested in [11, 20], stiffness of the surface is relatively low (260 N/m), but the damping term (130 Ns/m) provides rapid changes in force as surface contact is made, producing a surface that feels very hard when tapped, but which can be penetrated to several millimeters with constant pressure. This underlying "softness" is not easy to perceive, unless the user knows to look for it, because the kinesthetic sense cannot easily detect the small, slow displacements. The sharp force change upon contact is the dominant effect, causing the perceived surface to be very hard. Figure 14 shows the measured interaction forces and stylus positions during several taps on the virtual surface. Figure 15 shows a close-up of one of these contact events. Note the extremely fast changes in force as the wall is first penetrated. The forces also oscillate after contact, which may provide added realism, as many real surfaces produce similar contact forces [19]. Calculated Rate Hardness (from [11]) in N/s force change per m/s position change during initial surface contact is

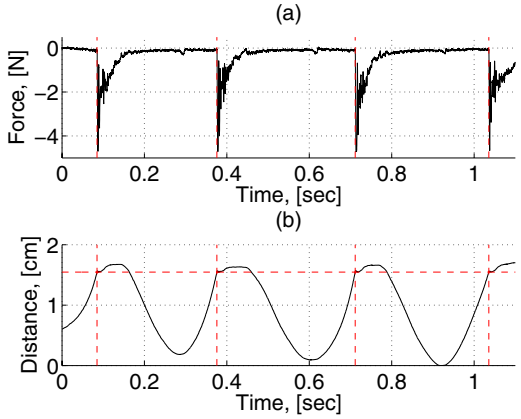

Figure 14: Interaction force and position data from tapping on the virtual surface.

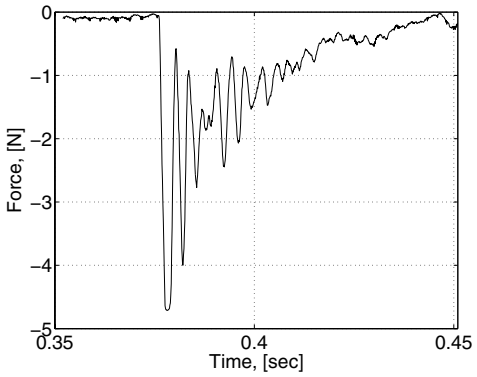

Figure 15: Close-up of a virtual wall contact event.

75,000 N/m, significantly larger than the 8,000 N/m and 10,000 N/m cases studied in [11], which users found difficult to distinguish. Athough not verified by psychophysical testing, this suggests that surfaces harder than shown in Figure 14 may not be perceptibly different, and the performance achieved by the bow spring/tendon actuator may be as high as necessary for high-quality hard surface rendering.

6 Conclusions and Future Work

A low cost bow spring/tendon actuator for haptic interfaces has been developed that is compact, yet provides a large range of prismatic motion. Actuator compensation techniques have been investigated that allow the use of inexpensive stepper motors and low line-count optical encoders in haptic interfaces. A combination of control system motion and force feedback compensation provides significant reduction of undesirable forces due to bow spring bias, Coulombic friction, and force ripple. The low mass and high stiffness bow spring/tendon connection to the user's fingers provides high fidelity rendering

Proceedings of the First Joint Eurohaptics Conference and Symposium on Haptic Interfaces for Virtual Environment and Teleoperator Systems
0-7695-2310-2/05 $20.00 © 2005 IEEE

of commanded forces, enabling both low free-space forces and high force rates-of-change for high-quality hard virtual surface rendering.

Future work will investigate the performance of a compact, multi-DOF haptic interface composed of parallel connections of the bow spring/tendon actuator elements to each end of a stylus handle.

References

[1] P. J. Berkelman and R. L. Hollis. "Haptic interaction using magnetic levitation", *Proc. ASME Int'l Mech. Eng. Congress, Dynamic Systems and Control Div.*, Anaheim, CA, Nov. 1998.

[2] M. Bodson, J. N. Chiasson, R. T. Novotnak, and R. B. Rekowski. "High-Performance Nonlinear Feedback Control of a Permanent Magnet Stepper Motor," *IEEE Trans. Control Systems Technology*, 1(1): 55–14, Mar. 1993.

[3] G. Burdea and J. Zhuang. "Dextrous Telerobotics with Force Feedback–an Overview," *Robotica*, Vol. 9, 1991.

[4] P. Buttolo and B. Hannaford. "Pen-Based Force Display for Precision Manipulation in Virtual Environments," *Proc. IEEE Virtual Reality Symposium*, pp. 217–224, 1995.

[5] J. Edward Colgate and J. Michael Brown. "Factors Affecting the Z-Width of a Haptic Display," *Proceedings of the IEEE International Conference on Robotics & Automation*, pp. 3205–3210, San Diego, CA, May 1994.

[6] M. Goldfarb and J. Wang, "Passive Stiffness Simulation with Rate-Independent Hysteresis", *Proc. ASME Dynamic Systems and Control*, DSC-Vol. 67, pp. 345–350, 1999.

[7] V. Hayward. "Toward a Seven Axis Haptic Device," *Proc. Int. Conf. Intelligent Robots & Systems*, 1995.

[8] D. Hughes and J. T. Wen, "Preisach Modeling of Piezoceramic and Shape Memory Alloy Hysteresis", *Proc. IEEE Conf. Control Applications*, Albany, 1995, pp. 1086–1091.

[9] H. Iwata. "Artificial Reality with Force Feedback: Development of Desktop Virtual Space with Compact Master Manipulator," *Computer Graphics*, 24(4), 1990.

[10] M. A. Krasnosel'skii and A. V. Pokrovskii, *Systems with Hysteresis*, Springer-Verlag, 1989.

[11] D. A. Lawrence, L. Y. Pao, A. M. Dougherty, M. A. Salada, and Y. Pavlou. "Rate-Hardness: A New Performance Metric for Haptic Interfaces," *IEEE Trans. Robotics and Automation*, 16(4): 357–371, Aug. 2000.

[12] C. D. Lee, D. A. Lawrence, and L. Y. Pao. "A High-Bandwidth Force-Controlled Haptic Interface," *Proc. ASME Dynamic Systems and Control Division*, DSC–Vol. 69–2, Orlando, FL, pp. 1299–1308, Nov. 2000.

[13] D. A. Lawrence, L. Y. Pao, A. C. White, and W. Xu. "Low Cost Actuator and Sensor for High-Fidelity Haptic Interfaces," *Proc. 12th Int. Symp. Haptic Interfaces for Virtual Environments and Teleoperator Systems*, *IEEE Virtual Reality Conf.*, Chicago, IL, pp. 74–81, Mar. 2004.

[14] C. D. Lee, D. A. Lawrence, and L. Y. Pao. "Isotropic Force Control for Haptic Interfaces," *Control Engineering Practice*, 12(11): 1423–1436, Nov. 2004.

[15] S.-H. Lee, T. J. Royston, and G. Friedman, "Modeling and Compensation of Hysteresis in Piezoceramic Transducers for Vibration Control", *ASME Adaptive Structures and Materials Systems*, AD-Vol. 59/MD-Vol. 87, 1999, pp. 11–18.

[16] G. Luecke and Y.-H. Chai. "An Exoskeleton Manipulator for Application of Electro-Magnetic Virtual Forces", *Proc. ASME Int'l Mech. Eng. Congress, Dynamic Systems and Control Div.*, Atlanta, GA, Nov. 1996.

[17] T. H. Massie and J. K. Salisbury. "The Phantom Haptic Interface: A Device for Probing Virtual Objects," *Proc. ASME Dynamics Systems and Control*, Vol. 1, pp. 295–301, 1994.

[18] H. Melkote and F. Khorrami. "Robust Nonlinear Control and Torque Ripple Reduction for Permanent Magnet Stepper Motors," *IEE Proc. Control Theory Appl.*, 146(2): 186–196, Mar. 1999.

[19] A. M. Okamura, M. R. Cutkosky, and J. T. Dennerlein, "Reality-Based Models for Vibration Feedback in Virtual Environments", *IEEE/ASME Trans. Mechatronics*, Vol. 6, no. 3, pp. 245–252, 2001.

[20] L. B. Rosenberg and B. D. Adelstein, "Perceptual Decomposition of Virtual Haptic Surfaces", *IEEE Symp. Res. Frontiers Virtual Reality*, San Jose, CA, Oct., 1993, pp. 46–53.

[21] S. E. Salcudean, R. Six, R. Barman, C. Jennings, S. Kingdon, D. Murray, and V. Tucakov. "Design Tradeoffs in the Development of a 6-DOF Desktop Haptic Interface," *Proc. ASME Int'l Mech. Eng. Congress, Dynamic Systems and Control Div.*, Anaheim, CA, Nov. 1998.

[22] R. L. Williams, II, "Cable Suspended Haptic Interface", *Proc. ASME Dynamic Systems and Control*, DSC-Vol. 64, pp. 207–212, 1998.

Proceedings of the First Joint Eurohaptics Conference and Symposium on Haptic Interfaces for Virtual Environment and Teleoperator Systems
0-7695-2310-2/05 $20.00 © 2005 **IEEE**